Chapter 5

Identical Particle Correlation Analysis

High energy heavy-ion collisions produce matter under extreme conditions of temperature and density. While the highest densities are reached in the early stages of the collision, most of the observed particles are hadrons which are emitted rather late in the evolution of the collision. Because of that the measured momentum spectra and correlations contain direct information only about the size, shape, and dynamics of the source at freeze-out. The two-particle Bose-Einstein interferometry is tool to study this information through the measurement of the relative momentum distribution of identical particles pairs. The analysis of three-dimensional correlation functions of like-sign π pairs, performed on the CERES data set, will be presented in this chapter. The Gaussian parameterization of the correlation functions, connecting the theory predictions with the experimental results, was performed in the Cartesian Bertsch-Pratt coordinate system (see Section 1.3.2). The 'out-side-long' components of the relative pair momentum four-vector were calculated in the Longitudinally CoMoving System (LCMS) in which the longitudinal component of the pair momentum vanishes.

5.1 Data Selection

The data set recorded in the year 2000 by the CERES experiment, after various calibrations, was used for the two-particle correlation analysis presented in this dissertation. Within this data set only the standard event cuts, namely the trigger event selection and the beam pile-up suppression, were performed. After high quality events were selected, every track used for the two-particle correlation analysis was subject to the following quality cuts:

- small χ^2 of the track fit (Fig. 5.1, left panel),
- at least 12 hits used in the fit (Fig. 5.1, right panel),
- fiducial acceptance cut $0.125 < \theta < 0.240$,

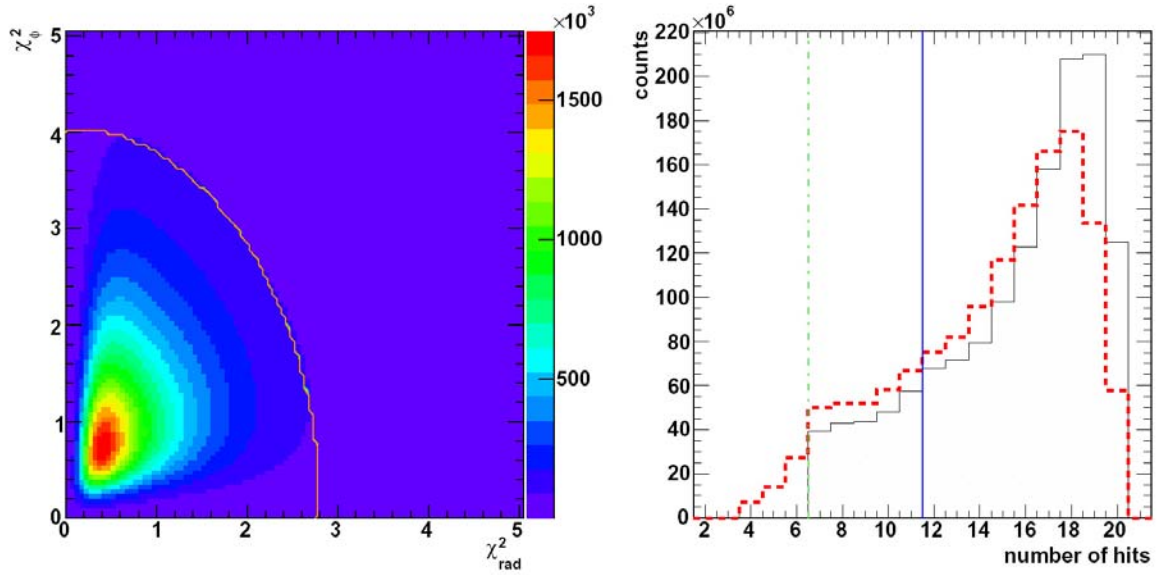

Figure 5.1: Left panel: the quality of the track fit in $r(t)$ and $\phi(z)$. The red line represents the cut. Right panel: distribution of the TPC track length: the total number of hits on track (black solid line), the number of fitted hits per track (red dash line). The vertical lines correspond to the cuts applied during the step2 production (dash-dot), and for the particle correlations analysis (solid).

- particle (pion-proton) identification based on the energy loss dE/dx versus track momentum (contours in Fig. 4.6),
- vertex cut (matching between SDD and TPC better than 2.5 σ) to suppress pions from K^0 and Λ^0 decays, as well as the protons coming from Λ^0 decays.

Since the time-space evolution of the colliding system strongly depends on the centrality of the collision the good knowledge of the event centrality is one of the important issues in the HBT interferometry. The relation between the measured event multiplicity and the impact parameter $\overrightarrow{b}$ is discussed in Section 4.8. Based on the fully calibrated information from the Multiplicity Counter seven centrality classes were selected for the two-particle correlation analysis. Table 5.1 summarizes the centrality selection.

While the pions from long-lived resonances like Λ^0 and K^0 can be significantly suppressed with a vertex cut the short-live resonances, which decay very close to their production point, could not be removed from the input data. Their most important effect is to lower the intercept of the correlation function (λ <1) [CL95, Hei96b, WH97].

The most important cuts in the two-particle analysis are the pair cuts. The finite granularity of the TPC resulted in the decrease of the reconstruction efficiency for very close tracks. Since

bin	$\sigma/\sigma_{\mathrm{GEOM}}(\%)$	$\langle\sigma/\sigma_{\mathrm{GEOM}}\rangle$ (%)	b_{min} - b_{max} (fm)	$\langle N_{part}\rangle$	$\langle N_{coll}\rangle$	$\langle\frac{dN_{ch}}{d\eta}\rangle\|_{\eta=3.1}$
1	< 2.5	1.28	< 2.4	366	850	428.3
2	2.5 - 5	3.74	2.4 - 3.3	325	781	389.9
3	5 - 7.5	6.10	3.3 - 4.1	298	666	356.2
4	7.5 - 10	8.06	4.1 - 4.7	274	643	330.5
5	10 - 15	11.65	4.7 - 5.8	234	522	288.1
6	15 - 25	17.49	5.8 - 7.4	180	345	230.4
7	25 - 35	29.98	7.4 - 8.8	124	224	142.9

Table 5.1: The centrality bins used in the analysis. The geometrical cross section for Pb+Au collisions σ_{GEOM} was assumed to be 6.94 b.

the track separation is related to the relative momentum between the two particles, and the effect mentioned above does not occur for the mixed pairs (background), the two-particle correlation function is strongly affected. Those pairs, for which the deflection in the magnetic fields brings the particles closer together, suffer more then the others. The two topologies, thus, have to be considered separately (Fig. 5.2). The selection between the so-called sailor and cowboy pairs was based on the condition

$$SC = (Q_1 \cdot Q_2)(Q_2 \cdot p_2 - Q_1 \cdot p_1)(\phi_2 - \phi_1) \tag{5.1}$$

where p_i=$|\overrightarrow{p_i}|$, Q_i, and ϕ_i are the momenta, charges, and azimuthal angles of the two particles (i=1,2), respectively. The positive and negative value of SC indicates, respectively, the sailor and the cowboy topology. The pairs, for which SC was equal to zero, were rejected. The efficiency, calculated as the ratio between the signal and the background pairs, is presented as a function of $\Delta\theta$ vs. $\Delta\phi$ for different pair transverse momenta in Fig. 5.3. This effect is corrected

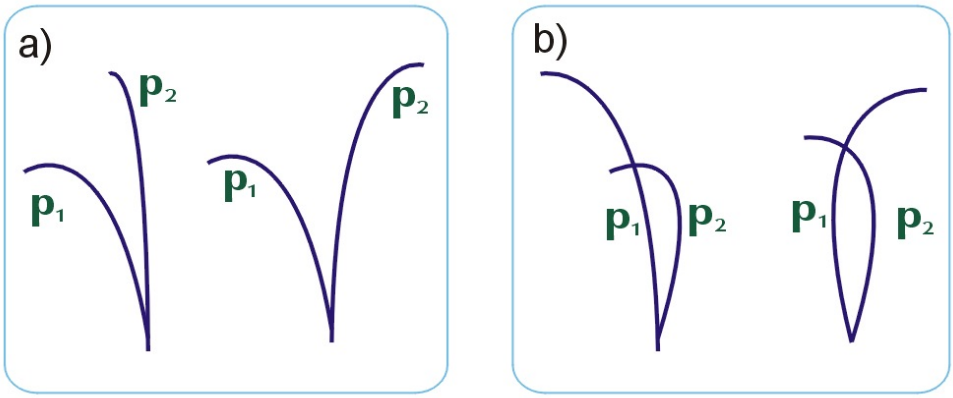

Figure 5.2: The different topology of pairs in the CERES TPC; a) sailors, b) cowboys.

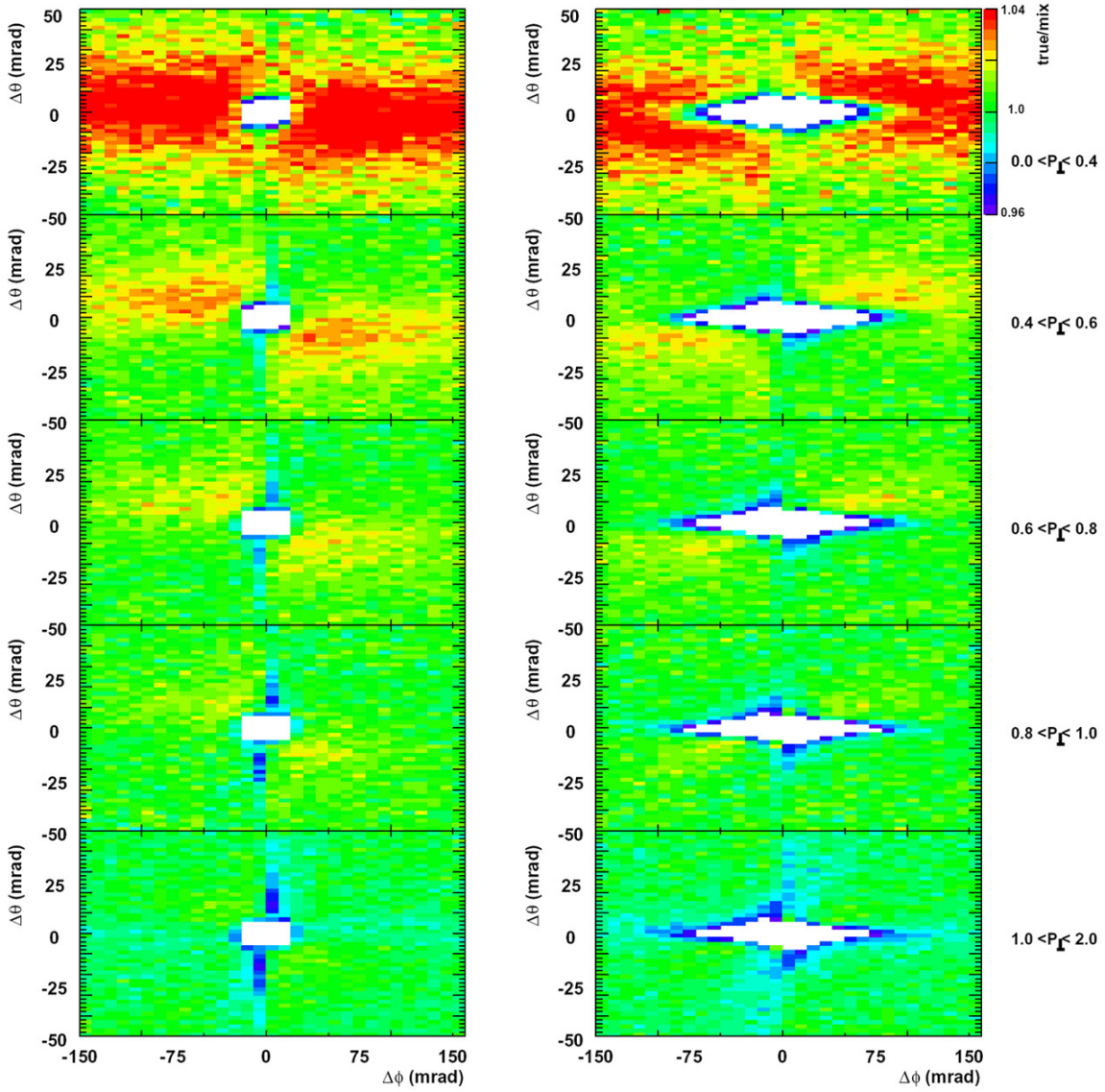

Figure 5.3: Two track resolution of the CERES TPC. Number of reconstructed track pairs, normalized to mixed events, $\Delta\phi$ and $\Delta\theta$ for the two pair topologies, sailor (left) and cowboy (right).

for by requiring a minimum opening angle between the tracks in a pair, both in the signal and in the background. The corresponding two-dimensional cuts were applied separately for a given pair topology, rapidity, and transverse momentum. The $P_\perp$-dependent separation cuts applied for the sailor pairs were varied between 8-9 mrad for $\Delta\theta$ and between 38-45 mrad for $\Delta\phi$. Small fluctuations in the $\Delta\theta$ around $\Delta\phi$=5 mrad were also removed. In the case of cowboy

pairs also so-called cross cuts were applied, however, with the much wider window in the $\Delta\phi$ (90-140 mrad).

Information concerning the dynamics of the relativistic heavy-ion collisions can be derived from the pair momentum dependence of the measured correlations functions. Therefore, the HBT analysis of the like-sign π was performed in eight bins of the transverse pair momentum ($P_{\perp,\pi\pi}$) defined by Eq. 1.10. The CERES experiment for the Pb-Au collision system at 158 GeV/c covered the backward Y region, close to the midrapidity $Y_B/2$=2.91. The results of many theoretical models are usually determined for the midrapidity region, hence the existed data set was divided into two bins of pair rapidity ($Y_{\pi\pi}$) in order to study qualitatively the rapidity dependence of the HBT parameters. In Fig. 5.4 the n($P_{\perp,\pi\pi}$, $Y_{\pi\pi}$) distribution of the π pairs with relative pair momentum below 150 MeV/c is shown. The horizontal and vertical lines represent chosen slices of $P_{\perp,\pi\pi}$ and $Y_{\pi\pi}$, respectively. Table 5.2 contains the mean values for each ($P_\perp$, Y) bin which were used for the representation of the HBT parameters vs. $P_\perp$ in the following chapter.

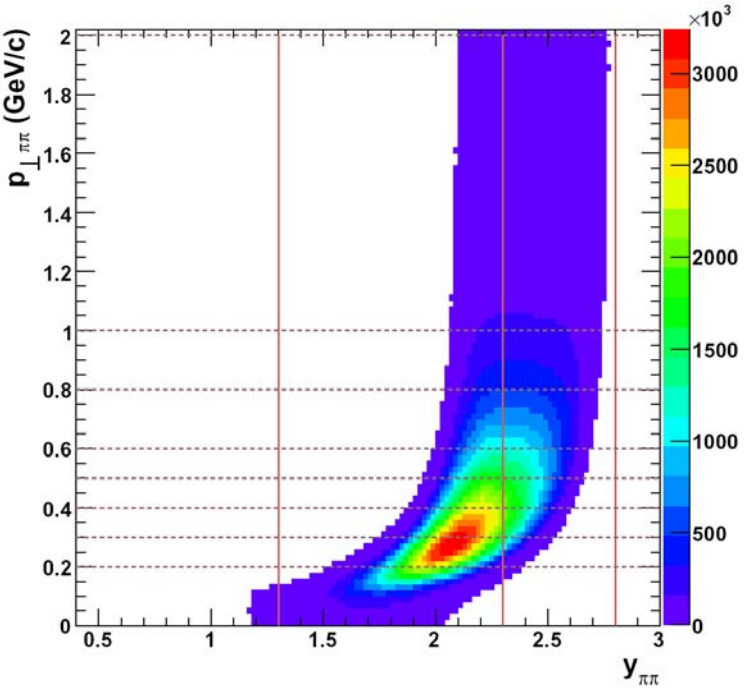

Figure 5.4: The like-sign pion pairs acceptance in the CERES TPC for pairs with relative momentum below 150 MeV/c. The horizontal and the vertical lines represent chosen cuts in the pair transverse momentum and in the pair rapidity, respectively.

pair	$Y_{\pi\pi}$ / $P_\perp$ bin (GeV/c)	0.0-0.2	0.2-0.3	0.3-0.4	0.4-0.5	0.5-0.6	0.6-0.8	0.8-1.0	1.0-2.0
$\pi^-\pi^-$	1.3-2.3	0.170	0.252	0.343	0.441	0.541	0.668	0.871	1.112
	2.3-2.8	0.190	0.282	0.362	0.452	0.548	0.681	0.876	1.119
$\pi^+\pi^+$	1.3-2.3	0.169	0.253	0.345	0.443	0.543	0.672	0.873	1.118
	2.3-2.8	0.190	0.283	0.363	0.453	0.549	0.683	0.877	1.127

Table 5.2: $P_\perp$ and Y intervals used in the analysis. For each bin the mean $P_\perp$ is given.

5.2 Definition of the Correlation Function

Experimentally, the two-particle correlation function for a given pair momentum **P** (see Eq. 1.9) and relative momentum **q** (see Eq. 1.11) is obtained by dividing the signal distribution $S(\overrightarrow{q}, \overrightarrow{P})$ by the reference or background distribution $B(\overrightarrow{q}, \overrightarrow{P})$ which should be ideally similar to the S in all respects except for the presence of femtoscopic correlations

$$C_2(\overrightarrow{q}, \overrightarrow{P}) = \frac{S(\overrightarrow{q}, \overrightarrow{P})}{B(\overrightarrow{q}, \overrightarrow{P})} \ . \tag{5.2}$$

In Fig. 5.5 an example of the signal and the background π pair distributions and the resulting correlation function is shown. Similarly, the three-dimensional like-sign π correlation functions were obtained using the 'out-side-long' components of the relative pair momentum vector calculated in the LCMS frame. Values of the relative momentum obtained in this frame were stored in three-dimensional histograms with a binning of 10 MeV/c for signal and background distributions. In order to correct for the final state Coulomb interaction between particles, an additional three-dimensional histogram of the same binning stored the Lorentz invariant four-momentum difference q_{inv} (see Eq. 1.12). The latter was used during the fit procedure of the correlation function as will be explained in Section 5.5.

5.3 Signal and Background Construction

The cuts, described in Section 5.1, were applied both for the signal and the background pairs. The signal $S(\overrightarrow{q}, \overrightarrow{P})$ refers to the relative momentum q distribution of two particles coming from the same event. The background distribution $B(\overrightarrow{q}, \overrightarrow{P})$ was obtained using pairs consisting of particles taken from two different events. Such method of background construction, commonly used in the data analysis of the high energy experiments, is called the event-mixing technique [Kop74]. In order to reduce the statistical uncertainties in the derived correlation functions the background was calculated from four additional events. The latter were chosen as an optimum between the computing time and the reduction of statistical errors. The background distributions should be indistinguishable from the signal distribution in all respects

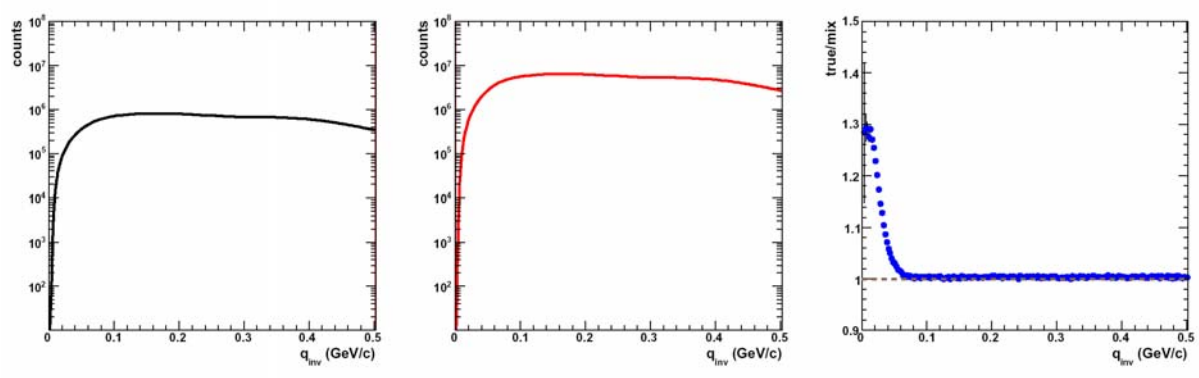

Figure 5.5: One-dimensional distribution of the momentum difference for the like-sign pion pair from the same event (left panel) and from different events (middle panel). The derived correlation function is shown in the right panel.

except for the presence of femtoscopic correlations. Therefore, each event was characterized by it centrality, vertex position, and the reaction plane orientation, and only events with similar properties were used to calculate the background distribution. The events were accumulated in ten bins of centrality. The bin width varied from 2 % $\sigma/\sigma_{\mathrm{GEOM}}$ for the most central collision region to 5 – 20 % $\sigma/\sigma_{\mathrm{GEOM}}$ in the case of more peripheral collisions. Moreover, events were split into eight classes of the reaction plane orientation angle Ψ_2, and only events coming from the same reaction target were mixed. This prevents the creation of an artificial structure in the correlation functions.

5.4 Fitting the Correlation

The three-dimensional correlation function for the like-sign particles can be parameterized by

$$C_2\left(\overrightarrow{q},\overrightarrow{P}\right) = N \cdot \left\{1 + \lambda\left(\overrightarrow{P}\right) \cdot \exp\left(-\sum_{i,j=1}^{3} R_{ij}^2\left(\overrightarrow{P}\right) q_i q_j\right)\right\}, \tag{5.3}$$

where N is a normalization factor and the correlation strength λ accounts for the long-lived resonances halo of the source distribution. The latter is also influenced by the detector resolution as well as by the misidentification of the particle species. The R_{ij}^2 parameters correspond to the Gaussian source radii derived in the 'out-long-side' coordinate system described in Section 1.3.2. The indices i, j run over three of the four components of q indicated as $out, long, side$.

Fitting the Eq. 5.3 to the derived correlation function based on the least square method and using the square root of the number of counts as an estimator of the error introduces a systematic bias by overestimating the significance of bin with a low number of counts [BC74]. The

maximum likelihood method, on the other hand, is free from this kind of bias. The MINUIT [MIN] package was used to minimize the negative logarithmic likelihood function

$$-2\log\mathcal{L}\left(R_{ij}^2\right) = 2\sum_b \left[C_2\left(R_{ij}^2\right)N_b - n_b\log\left(C_2\left(R_{ij}^2\right)N_b\right) + \log\left(n_b!\right)\right], \tag{5.4}$$

where n_b and N_b are the numbers of signals and background pairs in the relative momentum q bin b, and $C_2(R_{ij}^2)$ is the Gaussian parameterization of the correlation function. The last term in Eq. 5.4 does not depend on R_{ij}^2 and, consequently, can be neglected.

The correlation functions have to be corrected for the final state interaction of which the Coulomb interaction between charge particle is the most significant one. Therefore, the fit function was modified in order to account for such effect.

5.5 Coulomb Correction

Apart from Bose-Einstein statistics, correlations between like-sing charge particles occur by the final state interactions. The latter, due to repulsive interaction in the case of the like-sign particles, decrease the correlation strength and influence the width of the correlation function. In order to account for such effects different methods were tried. In the first approach the background distribution of the relative momentum difference was weighted with a correction factor characterizing the Coulomb repulsion. This over-corrects the correlation function since it neglects the fact that pions which come from long lived resonances do not feel Coulomb repulsion. A better method of removing the Coulomb effects from measured correlation functions was first suggested by [Bow91, S$^+$98] and then applied for the previous CERES analysis of the two particle correlation presented in [A$^+$03a]. The correlation function in this procedure was fitted by

$$C_2\left(\overrightarrow{q}\right) = N\cdot\left\{(1-\lambda)+\lambda\cdot F_c\left(q_{inv}\right)\left[1+\exp\left(-\sum_{i,j=1}^{3}R_{ij}^2 q_i q_j\right)\right]\right\}, \tag{5.5}$$

where $F_c\left(q_{inv}\right)$ is the squared Coulomb wave function described by Eq. 1.51 integrated over the emitting source. In this method the Coulomb term is coupled with λ to avoid the over-correction of the correlation function. The detailed description of deriving $F_c\left(q_{inv}\right)$ factors for different source size (in steps of 0.5 fm) used in this work is presented in Section 7.1. In Fig. 5.6 an example of one-dimensional projection of the three-dimensional correlation function together with both fits (Eq. 5.3 and Eq. 5.5) is shown. The projections $q_{out}, q_{side}, q_{long}$ of relative momentum vector decomposed in the Bertsch-Pratt coordinate system were produced for each component with an interval of $|q|$ <40 MeV/c in the other two directions. The difference between two fits reflects a Coulomb correction to the correlation function.

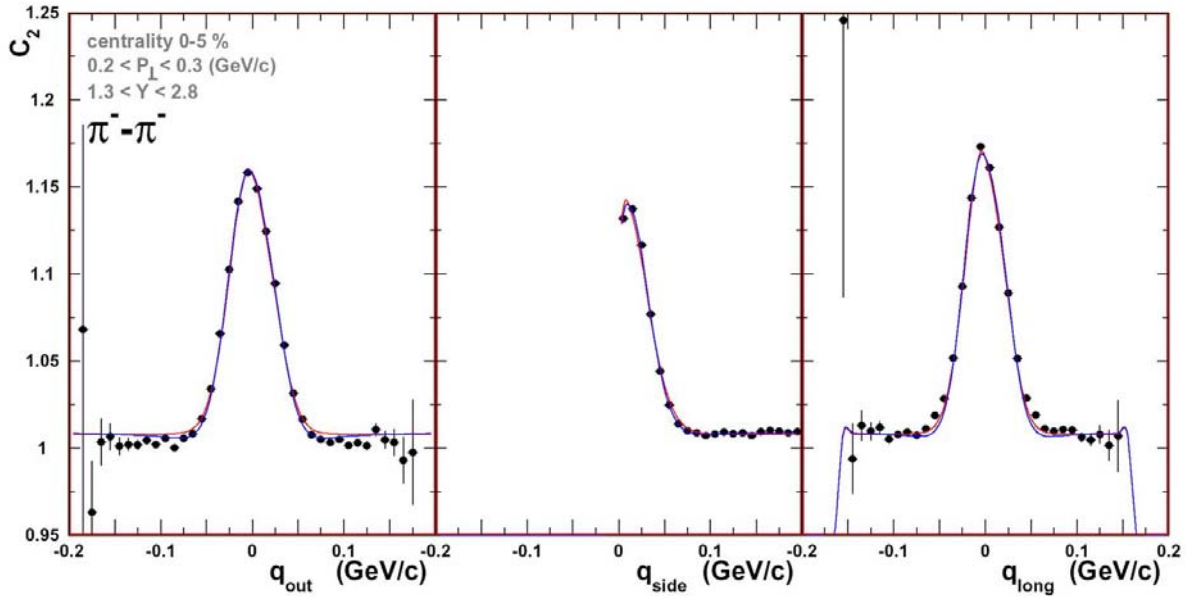

Figure 5.6: One-dimensional projection of the three-dimensional correlation function. The fit by Eq. 5.5 is depicted as the blue line, whereas the fit without the Coulomb correction shown by the red line.

The usually applied Gamow correction describes the square of the relative Coulomb wave-function of a particle pair at zero separation in the configuration space and thus does not take into account the finite source size. The effect of Gamow correction applied in its full strength or reduced by λ on the $\pi^-\pi^-$ correlation radii is shown as open triangles in the right and left column of Fig. 5.7, respectively. The results obtained with the finite-source Coulomb correction, calculated by averaging the squared Coulomb wave function over a Gaussian source distribution with $\sigma_x = \sigma_y = \sigma_z = 3$ fm and $\sigma_t = 0$ fm/c, are shown as full stars. The last method of Coulomb correction, depicted in Fig. 5.7 as full circle, consistently takes into account the actual size of the measured emitting source. The HBT radii dependence on the pair transverse momentum causes an under- or over-estimation of Coulomb interaction effects on the measured correlation functions when a constant source size Coulomb correction function is used for all $P_\perp$'s. Therefore, the measured one-dimensional HBT correlation function was used as an estimator of the emitting source size for a given $P_\perp$ bin. The one-dimensional function, similarly to the three-dimensional one, was fitted by

$$C_2\left(\overrightarrow{q}\right) = N \cdot \left\{(1-\lambda) + \lambda \cdot F_c\left(q_{inv}\right)\left[1 + \exp\left(-R^2 q^2\right)\right]\right\} \ , \tag{5.6}$$

where R reflects its size. The fit was done iteratively with the value of R, obtained from one iteration, used for the Coulomb correction in the next one. In first iteration the Coulomb correction factor was set to unity. The Coulomb correction factor obtained in such a way is

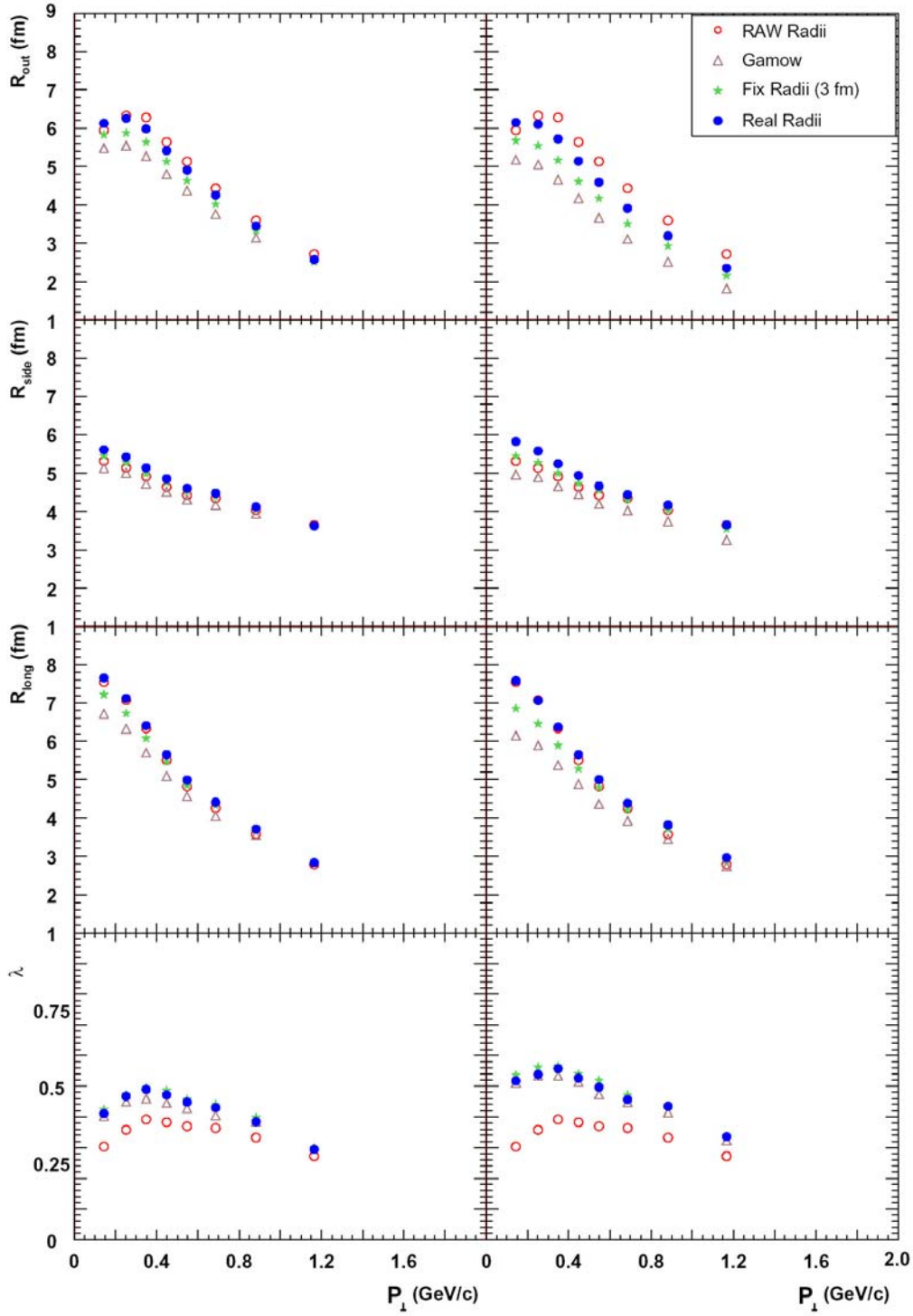

Figure 5.7: The $\pi^-\pi^-$ HBT radii as a function of the pair transverse momentum for different Coulomb correction methods. The HBT radii extracted from the three-dimensional correlation functions by Eq. 5.5 with different Coulomb corrections are shown in the left column. For comparison, the right column presents the HBT radii obtained with the full Coulomb strength. The data were not corrected for the detector resolution. The open red circles represents the uncorrected HBT radii (centrality bin 1-2).

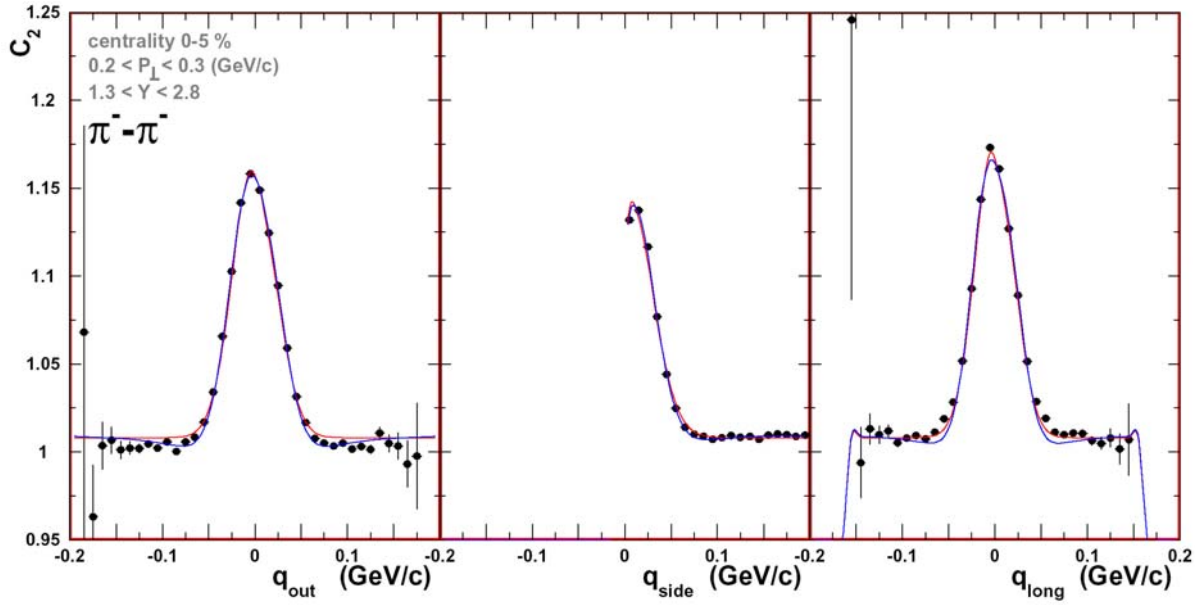

Figure 5.8: Results of the fit by Eq. 5.5 (blue line) with the parameterization of Coulomb interaction between like-sign particles based on the diluted Gamow factor. The red line shows the fit without Coulomb correction.

then used for the three-dimensional fit function. This was the method used to account for the effects of Coulomb interaction in the identical particle correlation functions considered in this dissertation.

A comparison between Figs. 5.6 and 5.8 shows that the phenomenological Coulomb correction can somewhat better describe the tails of $C(q_{out})$; it misses, however, the tails of $C(q_{long})$.

5.6 Transverse Momentum Dependence

In heavy ion collision an assumption of the static emitting source is certainly not an adequate one. The HBT radius parameters measure the size of the regions emitting particles of a given momentum (homogeneity regions) rather than the size of the fireball. The homogeneity radii depend on the velocity gradients and the temperature existing in the emitting source [WSH96, Wie98, TWH00]. This dependence is reflected in the measured correlation radii plotted as a function of the transverse momenta of the pairs of particles [Pra84, MS88] providing information about the dynamics of the matter created during the collision. Additionally to the $P_\perp$ dependence of the measured HBT radii the impact parameter significantly influences the extracted parameters. Therefore, a reasonably narrow centrality bins should be used while the

Bose-Einstein correlations are considered. In Fig. 5.9, like-sign pion HBT radii, uncorrected for the Coulomb interaction and detector resolution effects, are shown as a function of the transverse pair momentum for six different classes of centrality.

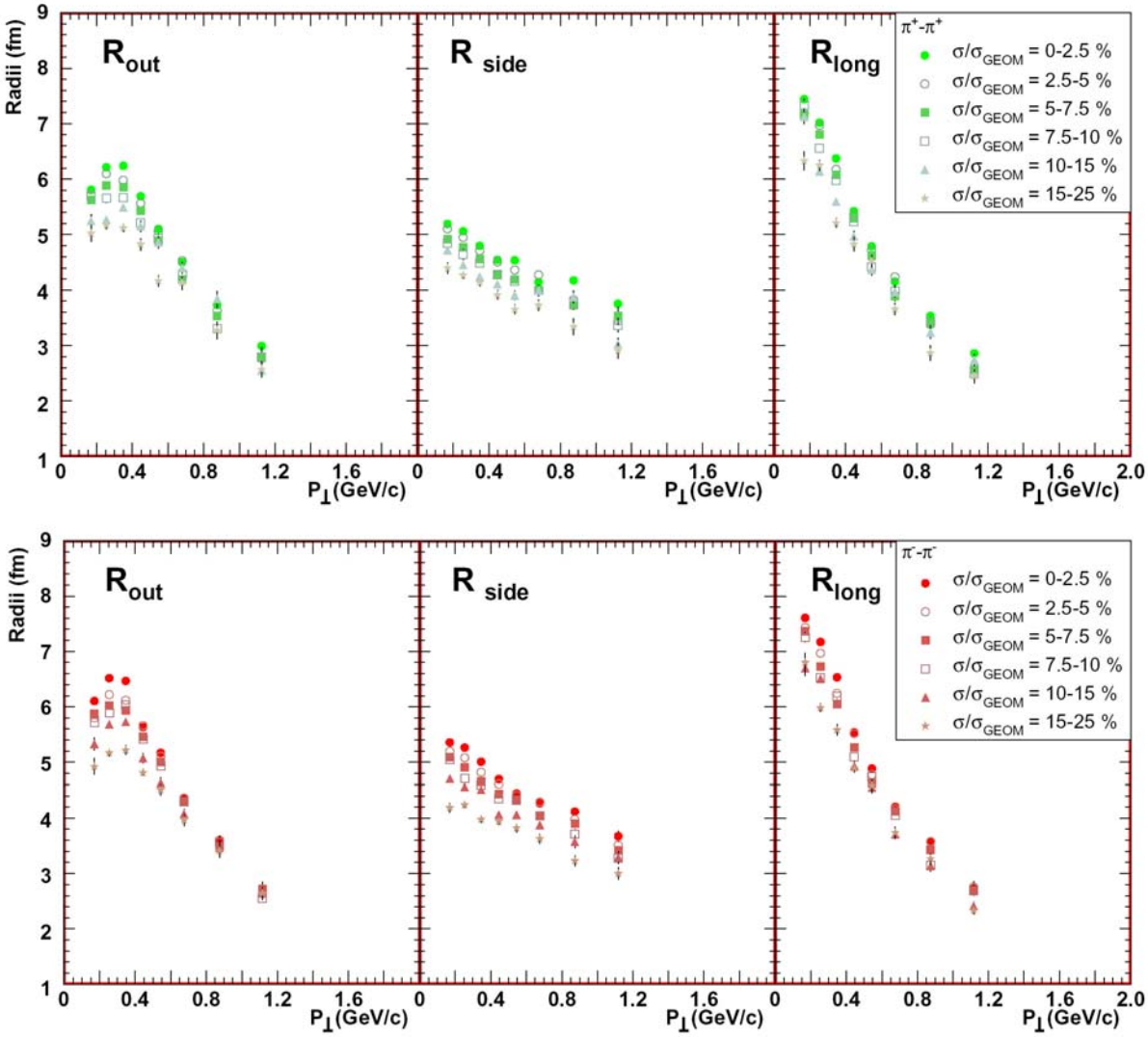

Figure 5.9: The transverse momentum dependence of the raw HBT radii, for $\pi^+\pi^+$ (top) and $\pi^-\pi^-$ (bottom).

5.7 Reaction Plane Orientation Dependence

Additional information concerning the dynamics of the emitting source can be obtained from non-central collisions, where freeze-out collision geometry might reflect the initial anisotropic almond shape, with its longer axis perpendicular to the reaction plane. Existence of the transverse pressure gradients in the reaction plane direction generated in such a colliding system leads to a preferential in-plane expansion [Oll92, KSH00] which diminishes the initial anisotropy as the system evolves. Therefore, the source shape at freeze-out should be sensitive to the evolution of the pressure and the system lifetime. Hydrodynamical calculations [KH03] predict that the source may still be out-of-plane extended after hydrodynamical evolution. However a subsequent rescattering phase tends to make the source in-plane extended [TLS01]. The study of HBT parameters relative to the reaction plane orientation in non-central collisions gives access to the spatial source anisotropy at freeze-out and might shared the light on different scenarios of the system's evolution.

The simple sketch of the method used to analyze the HBT radii relative to the reaction plane is shown in Fig. 5.10. The reaction plane orientation angle Ψ_2 was derived based on the Fourier expansion method explained in Section 4.7. Once the reaction plane is known one can calcu-

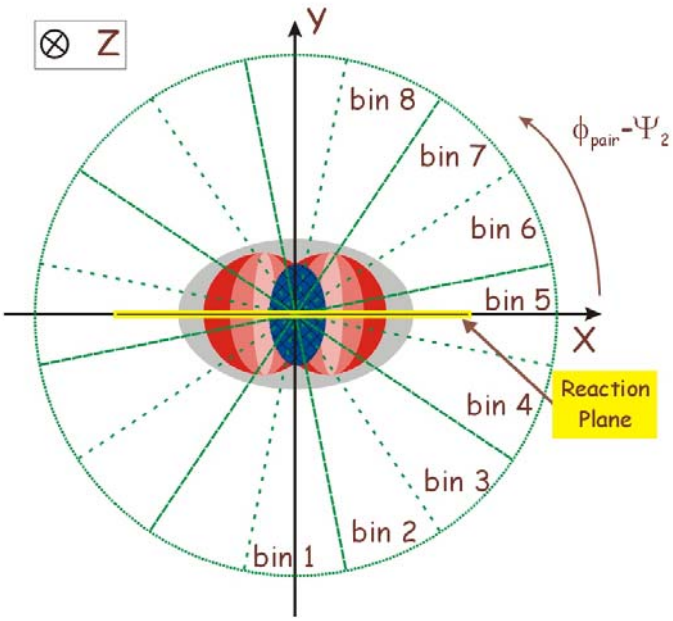

Figure 5.10: Sketch of the analysis method of the reaction plane dependent HBT radii. The space asymmetry in the collision is reflected in the momentum asymmetry of the produced particles depicted as a gray area. Two-pion correlation functions are analyzed separately for 8 bins of the azimuthal angle in respect to the reaction plane.

late the difference between the azimuthal orientation of a pair and the Ψ_2, $\phi_{pair} - \Psi_2$. Since the orientation of the reaction plane was calculated based on the second Fourier harmonics the information about the sign of the impact parameter vector is lost. In other words, the reaction plane angle is known modulo π. Therefore, due to the mirror symmetry with respect to the reaction plane only those space-time variance will not vanish which do not change the sign under $\Psi \rightarrow \Psi + \pi$ rotation. The analysis was performed in eight bins of the azimuthal angle difference $\phi_{pair} - \Psi_2$ in the transverse plane. For each bin a correlation function was constructed following the description presented in Section 5.2 for eight bins of $P_\perp$ and two bins of Y . Subsequently, the correlation functions were fitted with Eq. 5.5 and the derived HBT parameters were plotted as functions of the azimuthal angle difference. Since the observed anisotropies were hardly significant, and since, based on the blast wave calculations, not much $P_\perp$ was to be expected, all $P_\perp$ and Y bins were merged together before the fit was performed. Fig. 5.11 shows the measured dependence of the HBT radii on the azimuthal emission orientation not corrected for the finite reaction plane resolution and the finite binning in $\phi_{pair} - \Psi_2$. The dash line is a sine (cosine) fit to the HBT radii (cross-terms), comp. Eq. 5.5. The fit results are discussed in Section 8.2. The last point on all plots is identical with the first one and is omitted during the fit. The influence of the finite reaction plane angle resolution has a significant influence on the measured HBT radii. It decreases the measured amplitude of the HBT radii oscillations similarly as in the case of the elliptic flow [Oll98]. The correction for the reaction plane angle resolution will be discussed in Section 7.3.

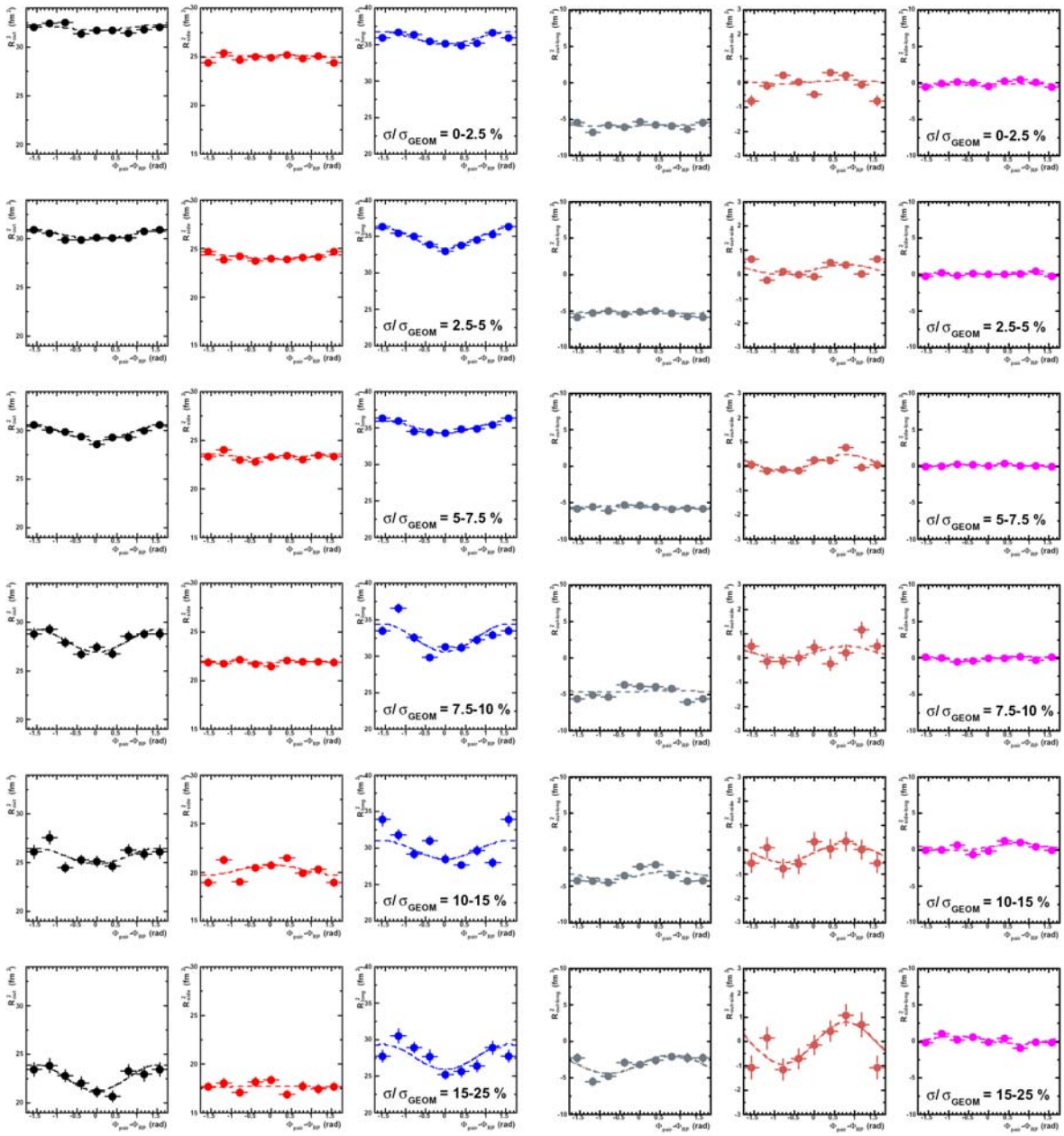

Figure 5.11: The reaction plane dependence of the HBT radii and the cross terms integrated over all bins of the pair $P_\perp$.

Chapter 6

Non-identical Particle Correlation Analysis

The correlations between non-identical same- and opposite-charge particles exhibit a minimum and a peak, respectively, at low relative momentum $\tilde{\mathbf{q}}$ (see Eq. 1.54), caused by the mutual Coulomb and the strong interactions. The small $\tilde{\mathbf{q}}$ implies that the two particles have the same velocity but not necessarily the same momenta. A difference between the average freeze-out position or time of the two particle species reveals itself as an asymmetry of the correlation function $C(\tilde{\mathbf{q}}, \mathbf{P})$ at small $\tilde{q}$ [LLEN96]. The asymmetry in the π-p correlations indicates that the proton source is located at a larger radius than the pion source or that protons are emitted earlier than pions [RftSC03]. This effect was attributed to the collective expansion of the system created during the collision i.e. to the transverse flow. In this chapter an analysis of π-p correlation functions will be presented. The analysis was performed in the Pair Center of Mass System (PCMS) in which the pair momentum vanishes. In this frame the relative momentum difference $\tilde{\mathbf{q}}$ is given by Eq. 1.11.

6.1 Analysis Variables and Frame

Two non-identical particle correlations were studied in the framework of the two-dimensional correlation functions $C(\mathbf{q}, \mathbf{P})$, defined by Eq. 5.2. The ratio of the signal distribution $S(\mathbf{q}, \mathbf{P})$ to the background distribution $B(\mathbf{q}, \mathbf{P})$ was constructed in the same manner as described in Section 5.3. The tracks chosen for the analysis were selected based on the set of cuts presented in Section 5.1, also the two-track resolution effect was treated in the same way as described in the case of the Bose-Einstein correlations. The experimental two-track resolution in general should affect less the non-identical particle correlation since pions and protons emitted with similar velocities have very different momenta in the laboratory frame. The correlation functions were calculated for $\pi^-\pi^+$, $\pi^- p$, and $\pi^+ p$ pairs in five bins of pair transverse momentum. The $\pi^-\pi^+$

correlation functions were calculated in order to cross-check the analysis method, since the correlation function for this combination is expected to be symmetric. The acceptance of the CERES experiment for the pion-proton pairs with the relative momentum below 150 MeV/c is shown in Fig. 6.1, where the horizontal and the vertical lines represent the chosen bins of $P_{\perp\pi-p}$ and $Y_{\pi-p}$, respectively. In order to increase the statistics, the data were integrated over the centrality and the pair rapidity bins. The analysis performed in centrality bins does not exhibit any differences between results obtained for those integrated over all centrality bins within statistical uncertainty. Table 6.1 contains the mean values of the pair transverse momentum in the laboratory frame integrated over rapidity intervals. By convention, **q** is calculated as a difference between momentum of the heavier and momentum of the lighter particle in the laboratory frame. The pairs are boosted to the pair centre of mass frame with $\overrightarrow{\beta} = \frac{\overrightarrow{P}}{E_{pair}}$. In this reference frame, the q vector is decomposed into the $q_{\parallel}$ and $q_{\perp}$ defined as

$$\begin{aligned} q_{\parallel} &= q_{out}\,, \\ q_{\perp} &= \sqrt{q_{side}^2 + q_{long}^2}\,, \end{aligned} \tag{6.1}$$

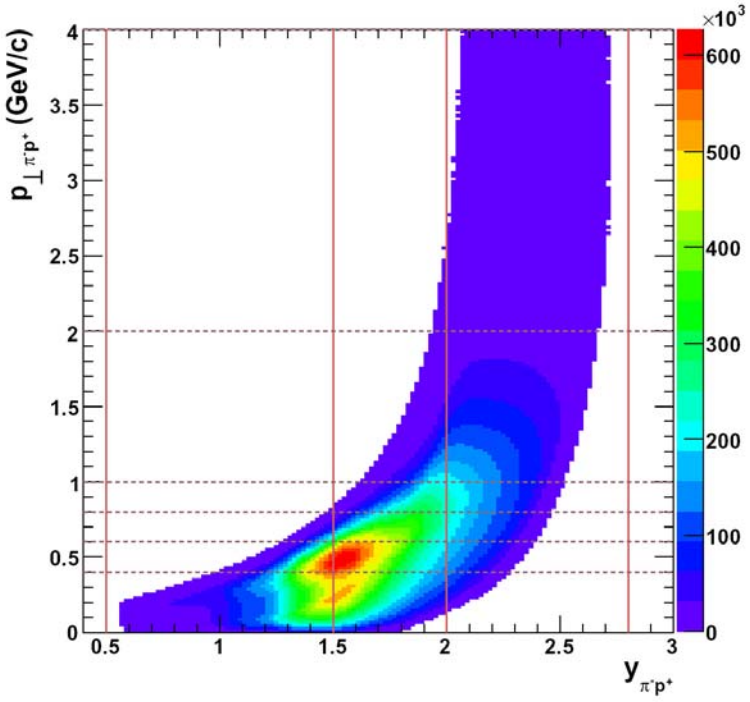

Figure 6.1: CERES acceptance for pion-proton pairs with the relative pair momentum below 150 MeV/c. The vertical and the horizontal lines represent the bins in the pair rapidity and in the pair transverse momentum, respectively.

pair	$P_\perp$ bin (GeV/c)	0.0-0.4	0.4-0.6	0.6-0.8	0.8-1.0	1.0-2.0	2.0-4.0
$\pi^- p^+$	$< P_\perp >$	0.286	0.507	0.685	0.885	1.214	2.185
$\pi^+ p^+$	$< P_\perp >$	0.287	0.508	0.686	0.884	1.215	2.189

Table 6.1: The different $p_\perp$ intervals used in the analysis of the non-identical particle correlation together with their mean $p_\perp$ values.

where q_{long} is the component parallel to the beam direction z, q_{side} is perpendicular to the beam direction and to the transverse pair momentum, and q_{out} is perpendicular to q_{long} and q_{side}. The q_{long}, q_{side}, and q_{out} are the well known variables of the Bertsch-Pratt parameterization but calculated in the analysis frame (PCMS). While the q_{out} is parallel to the transverse pair velocity and sensitive to the average separation of particles in the transverse direction, the q_{side} component should not show such effects. A similar analysis can be performed for the longitudinal direction, based on the sign of the q_{long} component as presented in [Miś98]. In Fig. 6.2 (left panel) an example of the two-dimensional correlation function $C(q_\perp, q_\parallel)$ for $\pi^- p$ pairs is shown. The convention chosen in the calculation of the relative pair momentum means that for $q_\parallel > 0$ ($q_\parallel < 0$) the lighter particle transverse velocity is smaller (larger) than the heavier one's. Therefore, the pion-proton correlations will be stronger when $q_\parallel < 0$ than when $q_\parallel > 0$, since in the first case pions tend to catch up with protons while in the second case pions tend to move away from protons (see Fig. 1.6).

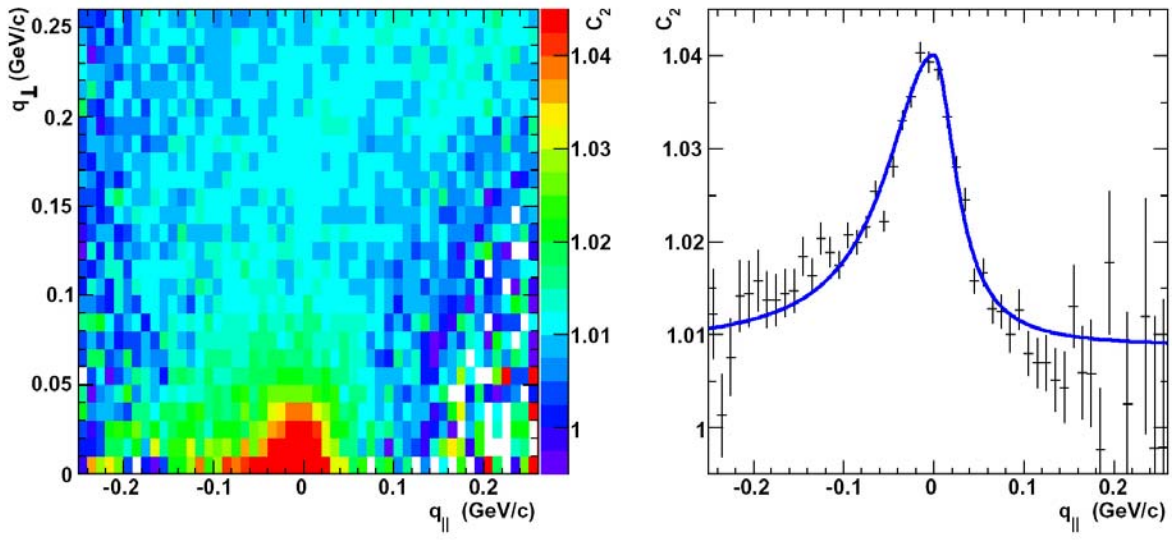

Figure 6.2: An example of the two-dimensional correlation function for π^--p^+ pairs (left panel). In the right panel the projection on the $q_\parallel$ axis with $q_\perp \in \{0, 50\}$ MeV/c and the fit by Eq. 6.2 is shown.

6.2 Parameterizing the Asymmetry of the Correlation Peak

The two-particle correlation functions for $\pi^-\pi^+$, π^-p, and π^+p pairs are caused mainly by Coulomb interaction. One should therefore, expect that the correlation effect will be positive for the unlike-sign pairs and negative for the like-sign ones. The derived experimental correlation functions confirm this expected behavior. Moreover, the peak (dip) in the pion-proton correlation function seems to be asymmetric. In order to qualitatively parameterize the asymmetry the signal and the background distributions were projected along $q_\perp$ within $\{0, 50\}$ MeV. Subsequently, the derived projection of the signal was divided by the projection of the background distribution, and a one-dimensional correlation function was obtained. The latter can be reasonably well described by a Lorentz curve with two widths σ_+ and σ_- given by

$$C_2(q_\parallel) = \begin{cases} N \cdot \left(1 + \frac{a}{\left(q_\parallel/\sigma_-\right)^2+1}\right), & q_\parallel < 0 \\ N \cdot \left(1 + \frac{a}{\left(q_\parallel/\sigma_+\right)^2+1}\right), & q_\parallel > 0 \end{cases} \tag{6.2}$$

where N is a normalization factor, and a corresponds to the peak amplitude. The asymmetry is then defined as the ratio between the two obtained widths ($\mathcal{A} = \sigma_-/\sigma_+$). In Fig. 6.2 (right panel) the fit to the one-dimensional correlation function is shown.

Two methods of quantifying the asymmetry are compared in Fig. 6.3. The originally proposed method, based on the one-dimensional correlation functions [LLEN96], is depicted as brown triangle while the method proposed in this dissertation is presented by the red circles. The correlation functions were calculated based on the Monte Carlo generator for a constant displacement of 6 fm in the transverse direction between π-p. The detailed description of the methods of constructing correlation functions is presented in Section 7.4. Following the original proposal, the ratio between the one-dimensional correlation functions $C_{2,+}$ and $C_{2,-}$ defines the mean distance between the two particle species at freeze-out. The C_2^- and C_2^+ were obtained using pairs with $q_\parallel < 0$ and $q_\parallel > 0$, respectively. If at any value of q the ratio C_2^-/C_2^+ differs from unity the asymmetry is observed. The sign of the deviation depends on the convention in the calculation of the relative momentum difference between particles as it was already mentioned before. The quality of both methods can be judged by comparing the fit parameter of Eq. 6.2. The fitted curve describes reasonably well the simulated correlation functions. Based on the definition of the $\mathcal{A}$ parameter the significance of a method can be expressed by

$$G_\mathcal{A} = \frac{\mathcal{A} - 1}{\delta\mathcal{A}}\,. \tag{6.3}$$

The ratios of the derived correlation functions are plotted in the left bottom panel of Fig. 6.3. The difference of the two histograms reflects the quality of the analysis method. In the case of the two-dimensional method the deviation from unity is larger, so it, should be more sensitive to the displacement between the sources of the two particle species. On the other hand, taking

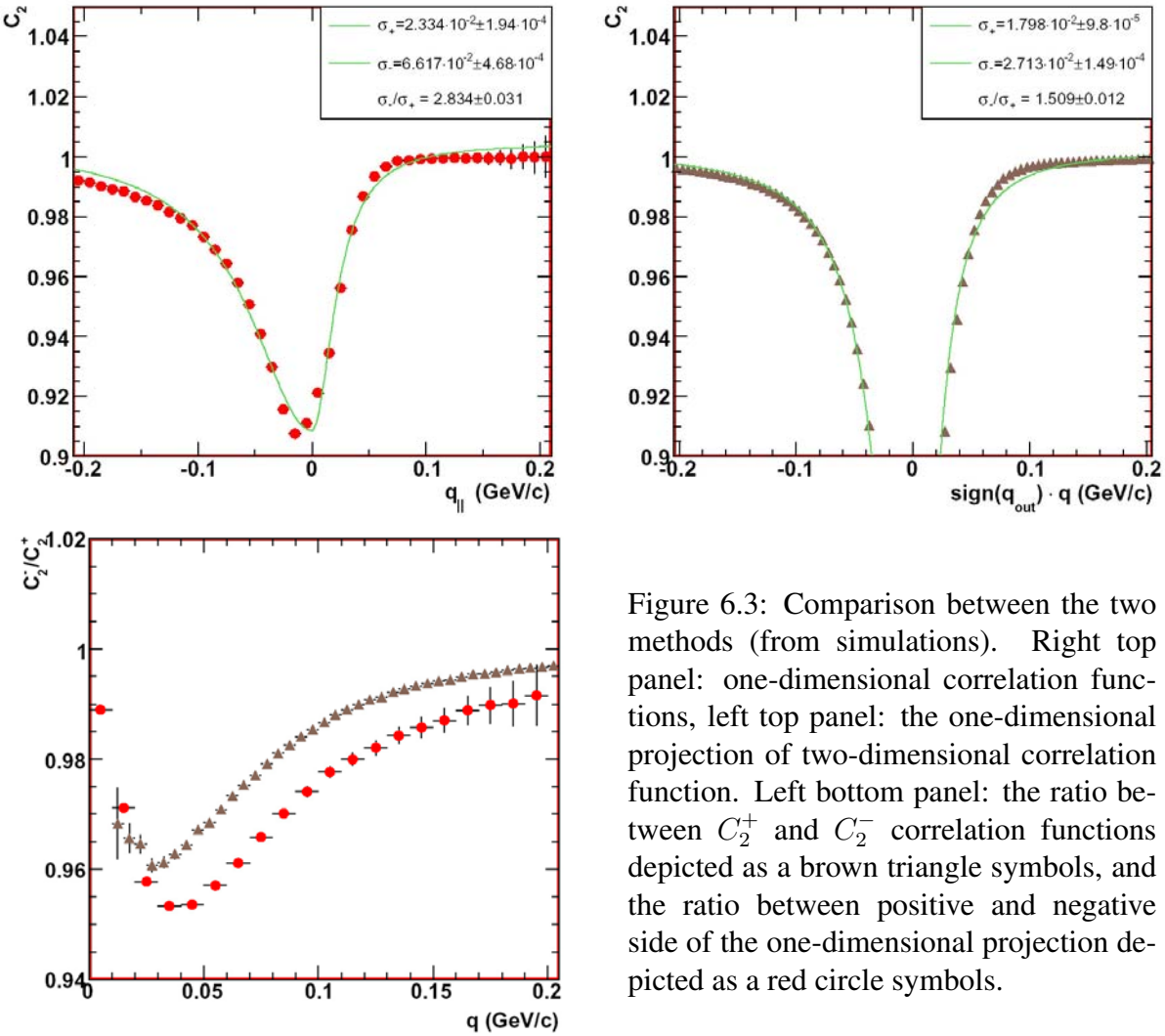

Figure 6.3: Comparison between the two methods (from simulations). Right top panel: one-dimensional correlation functions, left top panel: the one-dimensional projection of two-dimensional correlation function. Left bottom panel: the ratio between C_2^+ and C_2^- correlation functions depicted as a brown triangle symbols, and the ratio between positive and negative side of the one-dimensional projection depicted as a red circle symbols.

only the $q_\perp < 50$ MeV slice rather the entire space leads to larger statistical error bars. The quantitative comparison in terms of significance is presented in Table 6.2. The significance of the two-dimensional method is better by 40%. With the same procedure performed on the experimental correlation functions (see Fig. 6.4) this difference drops to about 8%. Inspecting Fig. 6.3 it can be seen that the fit by Eq. 6.2 did not entirely follow the shape of data points, therefore, it is foreseen to be use a two-dimensional fit instead of.

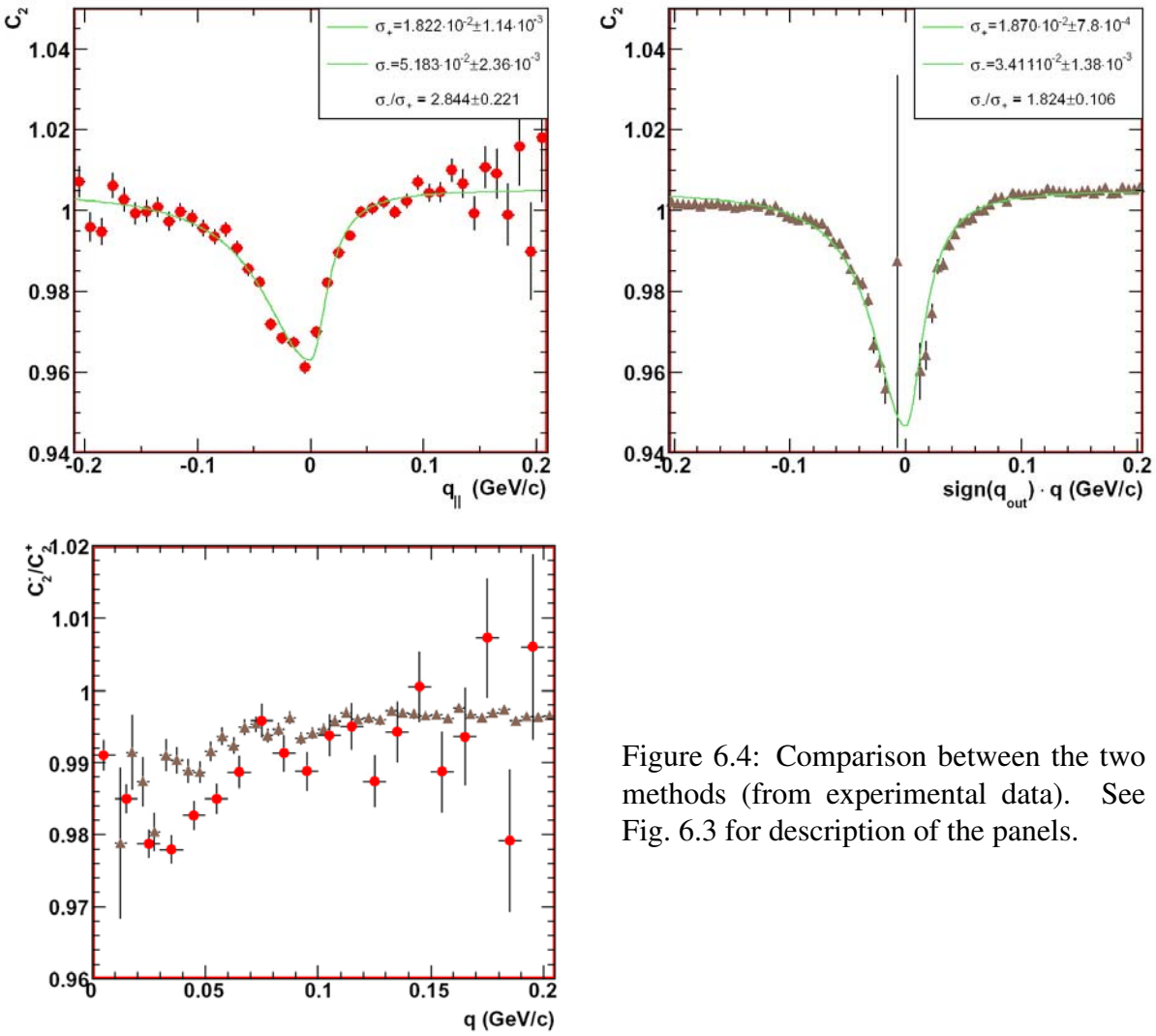

Figure 6.4: Comparison between the two methods (from experimental data). See Fig. 6.3 for description of the panels.

method	1 D	2 D
simulation	42	59
exp. data	7.77	8.35

Table 6.2: The significance of both methods.

6.3 Transverse Momentum Dependence

The displacement between the sources of different particle species from a system with collective expansion will arise naturally due to space-momentum and space-time correlation results in a collective velocity pointing outwards, added to the thermal velocities of the particles. The ve-

locity profile is such that the velocity is zero at the center (as it must be, for symmetry reasons) and maximum at the edge. To form a pion-proton pair with similar velocities a slow pion and a fast proton are needed, the latter coming preferentially from the edge of the fireball and thus profiting from a large velocity boost. This schematic explanation of the origin of the observed pion-proton asymmetry implies that the effect should disappear in the limit of zero pair momentum. The asymmetry as a function of the transverse momentum is shown in Fig. 6.5. The full symbols were obtained from the π^+-p$^+$ (square) and from the π^--p$^+$ (circle) correlations. The open triangles depicted the results of the unlike pion correlation functions. As expected from the symmetry consideration for the $P_\perp = 0$ the difference between emission time or emission position seems to vanish ($\mathcal{A} \to 1$). In order to study the asymmetry as a function of the displacement between particle sources a Monte-Carlo generator was used to translate $\mathcal{A}$ values to the displacement expressed in femtometers. The description of the method used to translate between these two different variables and the obtained results are presented in Sections 7.4 and 8.3.

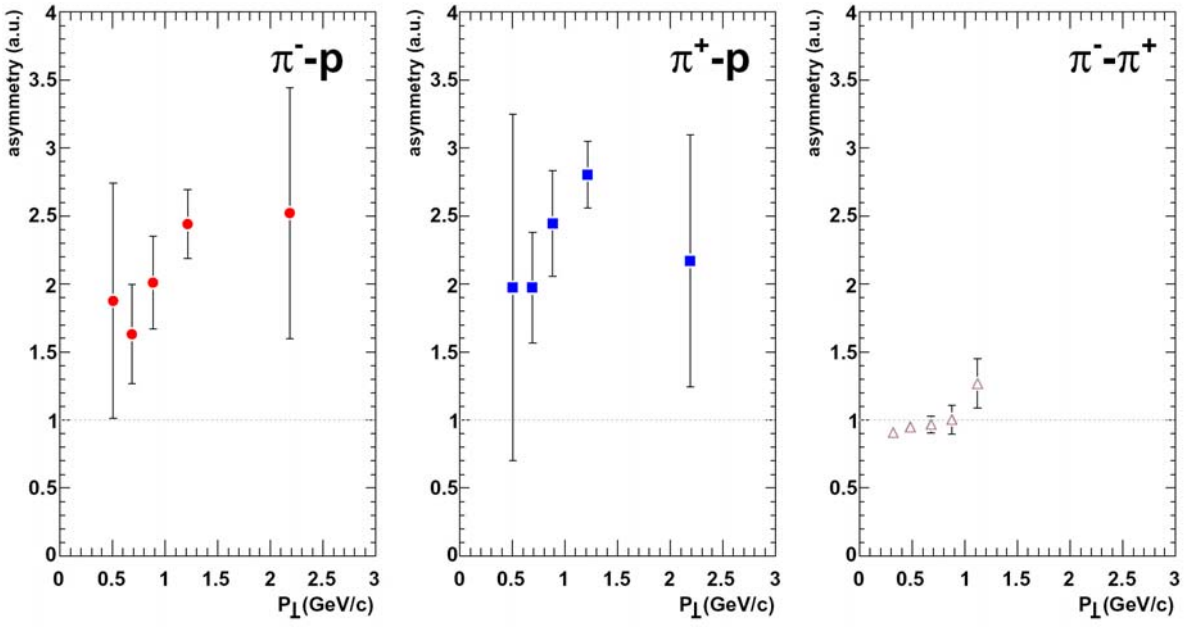

Figure 6.5: The source displacement as a function of the pair transverse momentum represent by the asymmetry variable.